Optoelectronic Readout of STT-RAM Based on Plasmon Drag Effect

Parinaz Sadri-Moshkenani, Mohammad Wahiduzzaman Khan, Md Shafiqul Islam, Eric Arturo Montoya, Ilya Krivorotov, *Senior Member, IEEE*, and Ozdal Boyraz

***Abstract*— An opto-electronic readout of the memory state in spin transfer torque random access memory (STT-RAM) cells is proposed. A single optical beam illuminating an array of STT-RAM cells creates electrical potential along each STT-RAM cell due to optical rectification that can be further enhanced through plasmon drag effect (PLDE). Then, the photo-induced voltage is assumed to be measured by conventional electronics. Here, a theoretical modeling is performed, where the results provide an estimate of the photo-induced voltage in each memory cell and its variation with respect to the changes in state of the memory cell (parallel vs anti-parallel). Our study shows that the plasmonic enhancement facilitates ∼*20* times enhancement in the voltage change due to state change of the each memory cell, compared to the case of out-of-resonance excitation. This enhancement potentially improves the memory readout rate if a proper supporting electronic circuit is available.**

***Index Terms*— Surface plasmons, plasmon drag effect, optical rectification, spin transfer torque random access memory, opto-electronic readout.**

I. INTRODUCTION

READOUT of state of random access memory (RAM) cells can be performed by electronic or optical means [1]–[6]. In specific, optical methods are advantageous for RAM readout, as they improve the memory performance, facilitate increased data transfer rate between processors and memory cells, and simplify the readout circuitry. The main challenge in optical readout systems arises from the fact that light sources and detectors are based on III-V materials [1], [2], [5], that are conventionally considered to be incompatible with CMOS foundries. However, recent developments in silicon photonics that include silicon-based optical sources, detectors and optical components may mitigate this bottleneck [7]–[10].

New memory technologies that allow high density memory cells, high speed, and low power read and write abilities are another subject that has been studied extensively. Among various types of RAM, spin transfer torque random access memory (STT-RAM) has received considerable attention due to its scalability (switching current decrease with memory cell width reduction), low power consumption ($100\,fJ$ per switch), high speed (read and write speed of $1\,ns$ to $10\,ns$), and high endurance [11]–[13]. The conventional method for STT-RAM readout is to measure the tunnel magnetoresistance, using an electronic readout circuit [4], [12], [14], [15]. However, up to date no study on its potential optical readout methods has been provided.

In this manuscript, we propose and study a potential optoelectronic readout method based on optical rectification (OR) and its plasmonic enhancement in metallic films in STT-RAMs [16], [17]. This method brings in the improvements of optical readout mentioned earlier without using conventional photodetectors.

The configuration we propose for this method is a parallel readout where an array of STT-RAM cells is illuminated by a pulsed laser beam (Fig. 1(a)). As a result of the optical illumination, an optical rectification voltage (OR voltage) is induced across each memory cell. We show that the magnitude of the OR voltage in each cell depends on the memory state of that cell. Therefore, it can be used as a means to detect the memory cells state (parallel (P) vs anti-parallel (AP)). This eliminates the need for electrical injection of current into the memory cells. Given that STT-RAM typically includes layers of plasmonic metal as electrodes [12], it is possible to facilitate the excitation of plasmonic modes in its structure. Previously we have shown that strong plasmonic field localization in STT-RAM multilayer is very sensitive to changes in its structure [18]–[20]. Here, we utilize similar effect to enhance the OR voltage and its sensitivity to changes in state of the memory cell, a phenomenon known as plasmon drag effect (PLDE) [21]–[23]. This in turn facilitates enhancement of memory readout rate. Our calculations show that if accompanying electronic circuit support it, the proposed readout method based on OR voltage with plasmonic enhancement can achieve up to more than 400 times increase in readout speed, compared to the case where the system operates at off resonance and does not take advantage of the plasmonic resonance.

In what follows, we first discuss the excitation of a localized plasmon resonance (LSPR) mode in STT-RAM cells. Next, we explain our model for calculation of the OR voltage with and without plasmonic enhancement, and also based on the state of the STT-RAM cell. Afterwards, we investigate the effect of dimensions of the STT-RAM memory cell on the

Manuscript received June 13, 2021; revised September 1, 2021; accepted September 7, 2021. Date of publication September 14, 2021; date of current version September 27, 2021. This work was supported by the Defense Threat Reduction Agency (DTRA) under Grant HDTRA1-16-1-0025. *(Corresponding author: Parinaz Sadri-Moshkenani.)*

Parinaz Sadri-Moshkenani, Mohammad Wahiduzzaman Khan, Md Shafiqul Islam, and Ozdal Boyraz are with the Department of Electrical Engineering and Computer Science, University of California at Irvine, Irvine, CA 92697 USA (e-mail: psadrimo@uci.edu; mohammwk@uci.edu; msislam1@uci.edu; oboyraz@uci.edu).

Eric Arturo Montoya and Ilya Krivorotov are with the Department of Physics and Astronomy, University of California at Irvine, Irvine, CA 92697 USA (e-mail: eric.montoya@uci.edu; ilya.krivorotov@uci.edu).

Color versions of one or more figures in this article are available at https://doi.org/10.1109/JQE.2021.3112701.

Digital Object Identifier 10.1109/JQE.2021.3112701

0018-9197 © 2021 IEEE. Personal use is permitted, but republication/redistribution requires IEEE permission.
See https://www.ieee.org/publications/rights/index.html for more information.

Authorized licensed use limited to: Access paid by The UC Irvine Libraries. Downloaded on December 07,2021 at 17:42:17 UTC from IEEE Xplore. Restrictions apply.

LSPR resonance and the potentially achievable memory readout rate. Finally, we study the effect of adding a transparent electrode, to accommodate probing of the memory cells.

II. Localized Surface Plasmon Resonance in STT-RAM Array

The main building block in the structure of STT-RAM is a magnetic tunnel junction (MTJ), consisting of a ferromagnet (CoFeB) / dielectric (MgO) / ferromagnet (CoFeB) multilayer stack, all placed between two metal layers as electrodes (Au) (Fig. 1(b)) [12]. Here, we focus on excitation of a localized surface plasmon resonance (LSPR) mode in each cell to enhance the OR voltage (V_{OR}). We choose LSPR because in comparison with surface plasmon polariton (SPP) modes, LSPR modes are more sensitive to the changes in the optical properties of materials, such as changes in optical properties due to the switching of memory state [24]. In addition, an LSPR mode enables interaction between light and individual memory cells without causing any cross coupling between adjacent memory cells. This makes the proposed method reliable for a cell-by-cell readout, instead of a collective response that an SPP mode would provide.

We design STT-RAM array structure resonant around 1.5 μm wavelength to study the optical rectification effect and its enhancement by LSPR excitation. To perform the numerical simulations for the STT-RAM array, COMSOL Multiphysics 5.6 is used, where a linearly polarized normally incident plane wave is defined as optical illumination, as illustrated in Fig. 1(b). Since the structure is symmetric, we simulate only half of the unit cell shown in Fig. 1(a), while using periodic and symmetry boundary conditions. As for the material data in our simulations, we take data for Au from [25], and we set the refractive index of MgO to 1.73 [26]. For the CoFeB layers, we use the thin-film material data provided in [27], which we extend to wavelengths larger than 1.6 μm via curve fitting. We assume that the material properties of all the layers are independent of their thickness.

To achieve plasmonic enhancement of the OR voltage and therefore enhanced memory readout speed, the STT-RAM array should be designed to support a plasmonic resonance with its maximum absorption at the design wavelength and a strong field localization in the MgO layer, where most of the resistance changes occur as the state of the memory switches. As a demonstration of such plasmonic resonance, we design an STT-RAM array with dimensions listed in the caption of the Fig. 1 to achieve an LSPR mode excitation at 1.5 μm. The main design parameters are the diameter of the nanodiscs in the structure of the unit cell (d), which tunes the resonance wavelength (wavelength at the peak absorption and highest field localization), and the unit cell period (p), which determines the fill factor of the memory cell and the resonance strength accordingly. We note that the thickness of the Au ground plane is fixed at $t = 100\,nm$ throughout this manuscript, which is much larger than the skin depth of gold ($\leq 23.5\,nm$) in the wavelength range of the simulations. Therefore, there is no need to include the underlying dielectric substrate in the simulations.

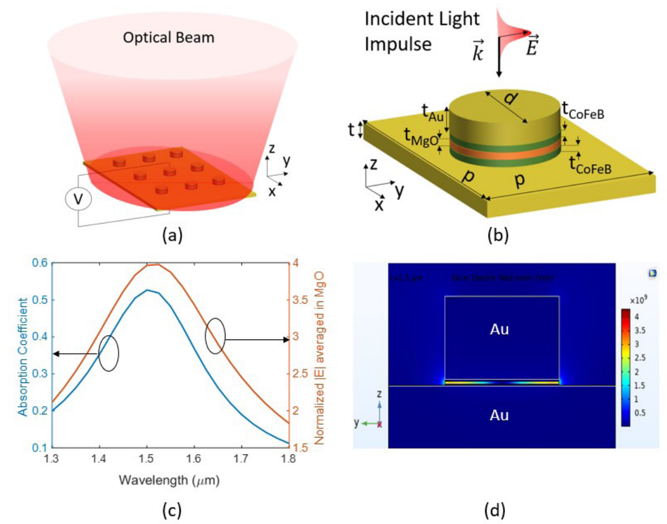

Fig. 1. (a) Schematic of the proposed optoelectronic readout method for STT-RAM array (b) Unit cell geometry of STT-RAM array (c) STT-RAM array spectra for optical absorption and average of electric field magnitude in MgO layer (d) Cross-sectional view of unit cell field distribution at resonance (STT-RAM array dimensions $p = 200\,nm$, $d = 100\,nm$, $t_{\mathrm{Au}} = 60\,nm$, $t_{\mathrm{CoFeB}} = 0.9\,nm$, $t_{\mathrm{MgO}} = 2\,nm$, $t = 100\,nm$).

Optical simulation results for the designed STT-RAM array are presented in Fig. 1(c), where the absorption spectrum shows a peak at the design wavelength. In addition, the plasmonic field localization is shown to be mainly in the MgO layer, as illustrated in Fig. 1(d). We also calculate the spatial average of electric field magnitude ($|E|$) throughout the MgO layer, normalized to the incident electric field (red curve in Fig. 1(c)), with its peak around the wavelength of the peak absorption. Therefore, one can use either the absorption coefficient or the normalized $|E|$ average in the MgO layer to determine the resonance in the design process. In the rest of the manuscript, we use the absorption coefficient to define resonance. The strong field localization in the MgO layer caused by the LSPR resonance helps enhance the change in the OR voltage due to the memory state change modeled as a material change in the MgO layer. Further details regarding the modeling of each memory state and calculation of V_{OR} are presented in the following section.

III. Calculation of OR Voltage in STT-RAM Array

Calculation of the OR voltage across each STT-RAM cell can be performed by adopting the formulation derived in [17], where the OR voltage for each cell is calculated as the time average of the photo-induced voltage (DC voltage) along z direction:

$$V_{OR} \approx \frac{1}{n^{(0)}q}\int \frac{dz}{A_z(z)}\Bigg[\int dA_z.(\frac{\alpha_R}{4}\nabla|\tilde{E}(z)|^2) + \frac{|\alpha|}{4}\langle|\tilde{E}(z^-)_\perp|^2\rangle_{A_z}\hat{n}(z).\hat{z}\Bigg] \quad (1)$$

Here, $n^{(0)}$ is the zeroth-order electron density in the metal layers, q is the electron charge ($1.6 \times 10^{-19}\,C$), α is the polarizability of the metal layer across which the voltage is induced, and α_R is the real part of it. $A_z(z)$ is the cross

Authorized licensed use limited to: Access paid by The UC Irvine Libraries. Downloaded on December 07,2021 at 17:42:17 UTC from IEEE Xplore. Restrictions apply.

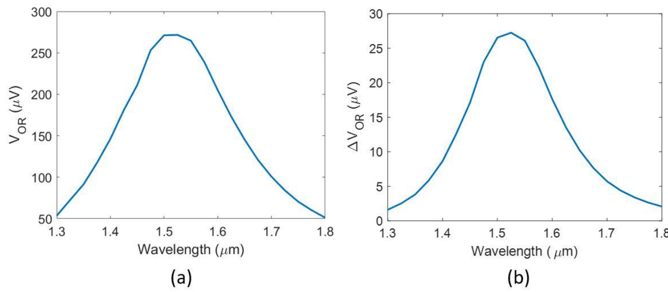

Fig. 2. (a) Calculated OR voltage for memory cell in STT-RAM array without taking the memory cell state into account (b) Calculated OR voltage change with the state change of memory cell for the STT-RAM array (STT-RAM array dimensions $p = 200\,nm$, $d = 100\,nm$, $t_{\text{Au}} = 60\,nm$, $t_{\text{CoFeB}} = 0.9\,nm$, $t_{\text{MgO}} = 2\,nm$, $t = 100\,nm$, laser incident peak power of $3\,kW$ and illumination beam spot size of $20\,\mu m \times 20\,\mu m$).

section of the metallic structure in xy plane at each z location, and $\hat{n}(z)$ is an outward unit vector perpendicular to the metal surface at each z location. Finally, $\tilde{E}(z)$ is the complex optical electric field vector, and $\tilde{E}(z^-)_\perp$ is the component of it perpendicular to the metal surface at a depth equal to Thomas-Fermi screening length of the metal (l_{TF}). For calculation of V_{OR} in one unit cell of STT-RAM array using equation (1), we use COMSOL Livelink with MATLAB to define several cut planes across the metal layers and capture the electric field data on them after running the numerical simulation and post-process it afterwards. For calculations in this paper, we use $n^{(0)} = 5.9 \times 10^{28}\,m^{-3}$ for Au, from which we calculate its screening length as $l_{TF} \approx \frac{1}{2}\left(\frac{a_0^3}{n^{(0)}}\right)^{1/6} = 0.583\,\text{Å}$, where a_0 is the Bohr radius [28], [29]. For CoFeB, we use $n^{(0)} = 17 \times 10^{28}\,m^{-3}$ and $l_{TF} = 1.3\,\text{Å}$, approximating by the parameters for Fe [30]. This is a reasonable approximation for the case of $Co_{20}Fe_{60}B_{20}$, which is one of the generic forms used in MTJ structures, mostly consisting of Fe [31].

To show the plasmonic enhancement of the V_{OR} in each memory cell of the STT-RAM array, we use equation (1) to calculate V_{OR} versus wavelength for one unit cell of the STT-RAM array with the same dimensions as mentioned in section II. We note that this calculation is performed assuming a pulsed laser with peak power of $3\,kW$ and a beam area of $20\,\mu m \times 20\,\mu m$ illuminating the STT-RAM array. Fig. 2(a) includes the result of such calculation, where V_{OR} reaches its maximum ($V_{\text{OR,max}}$) at the wavelength of plasmonic resonance at around $1.5\,\mu m$, confirming the contribution of such resonance in increasing V_{OR}.

Memory readout can be performed if we distinguish the state of the memory cells by using the OR voltage. To quantify this, we introduce the effect of memory cell state into our model by assigning a conductivity value to the MgO layer for each memory state. This is a valid assumption, since the conductivity values we use for STT-RAM in this manuscript, are more than three orders of magnitude smaller than the conductivity of CoFeB and Au [32], [33]. To calculate the MgO conductivity for each state (AP vs P), we use measurement data from [34], which reports values of resistance area (RA) product and tunnel magnetoresistance (TMR) ratio for a fabricated STT-RAM cell as $RA = 2.9\,\Omega\mu m^2$ and $TMR = 165\,\%$, respectively. Considering the 2 nm thickness of the MgO layer in our model, the conductivity assigned to MgO for parallel state would be $\sigma_P = t_{MgO}/RA \approx 690\,S.m^{-1}$. Using this and $TMR = (\sigma_P - \sigma_{AP})/\sigma_{AP}$, the MgO conductivity for anti-parallel state is calculated to be $\sigma_{AP} \approx 260\,S.m^{-1}$. By using these conductivity values for the MgO layer in our simulations, we calculate the OR voltage change caused by the memory state change ($\Delta \text{V}_{\text{OR}}$). The results are presented in Fig. 2(b), where the peak voltage change of the memory cell is $\Delta \text{V}_{\text{OR, max}} \approx 27.26\,\mu V$.

We can calculate the maximum potentially achievable memory readout rate for the designed STT-RAM array using the calculated ΔV_{OR} value. Since PLDE is an extremely fast phenomenon (femtosecond scale) [35], it can easily respond to an incident laser with MHz-range pulse repetition rate. However, to calculate the readout rate, one should consider the maximum laser pulse repetition rate allowed for differentiating between the two states of the memory cell and multiply it by the number of memory cells for which the readout is performed for each laser pulse. The maximum allowable laser pulse repetition rate can be calculated using the value of ΔV_{OR} obtained from the simulations, the noise equivalent power (NEP) of the system, including the noise from the readout circuit and the MTJ thermal and magnetic noise, and the desired signal-to-noise ratio (SNR) for the output signal. Using the calculated value of ΔV_{OR} and knowing the NEP of the system and the desired SNR at the output, the maximum allowable repetition rate of the pulsed laser can be determined by calculating the required detection bandwidth for detecting the voltage change as $BW = \frac{1}{SNR}\left(\frac{\Delta V_{\text{OR}}}{NEP}\right)^2$. Considering the $20\,\mu m \times 20\,\mu m$ spot size and the unit cell period of $200\,nm$ in our design, the proposed method can perform parallel activation of 10000 memory cells per laser pulse for the designed STT-RAM array. This may potentially contribute to a high memory readout speed. However, one should note that there will be limitations from the electronic circuit in the system in terms of maximum number of cells that can be measured in parallel due to the total noise performance of the system. In this manuscript, we focus on the optical rectification and its potential application to parallel activation of STT-RAM cells for fast read out. Hence, without making assumptions regarding the NEP value and maximum number of cells that can be electrically measured in parallel per laser pulse, here we focus on plasmonic enhancement of $\Delta \text{V}_{\text{OR}}$ and its contribution to the potentially achievable readout rate. For the designed STT-RAM array, such enhancement occurs around $1.5\,\mu m$ wavelength, shown in Fig. 2(b), providing a 288-fold increase in the potentially achievable readout rate compared to the off-resonance case of $1.3\,\mu m$ wavelength.

IV. Impact of Dimensions on OR Voltage

To increase V_{OR}, i.e. the potentially achievable readout rate, further, one can increase the incident peak power or engineer the STT-RAM dimensions. To demonstrate the impact of the power, we increase the incident power while keeping the illumination area the same, which means an increase in the incident intensity. Using the model explained in the previous

Authorized licensed use limited to: Access paid by The UC Irvine Libraries. Downloaded on December 07,2021 at 17:42:17 UTC from IEEE Xplore. Restrictions apply.

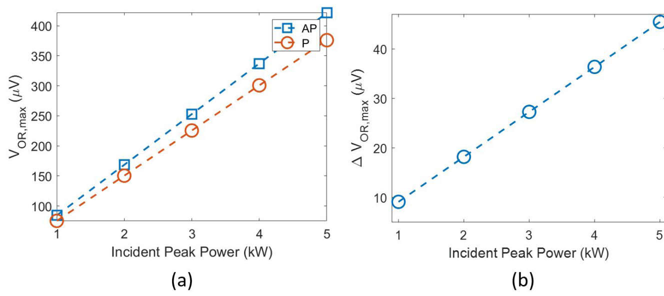

Fig. 3. Effect of changing the incident peak power upon the STT-RAM array on (a) Maximum OR voltage across each memory cell for parallel and anti-parallel memory states (b) Maximum OR voltage change with the state change of memory cell (STT-RAM array dimensions $p = 200\,nm$, $d = 100\,nm$, $t_{\text{Au}} = 60\,nm$, $t_{\text{CoFeB}} = 0.9\,nm$, $t_{\text{MgO}} = 2\,nm$, $t = 100\,nm$, illumination beam spot size of $20\,\mu m \times 20\,\mu m$).

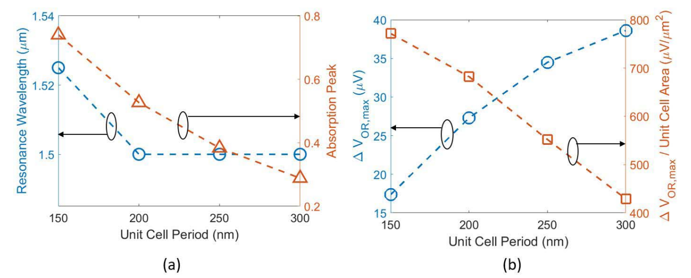

Fig. 4. Effect of changing the unit cell period of STT-RAM array on (a) Absorption peak and resonance wavelength (b) Maximum OR voltage change caused by the state change in each memory cell, and normalized $\Delta V_{\text{OR, max}}$ by the unit cell area (STT-RAM array dimensions $d = 100\,nm$, $t_{\text{Au}} = 60\,nm$, $t_{\text{CoFeB}} = 0.9\,nm$, $t_{\text{MgO}} = 2\,nm$, $t = 100\,nm$, incident peak power of $3\,kW$ and illumination beam spot size of $20\,\mu m \times 20\,\mu m$).

section, $V_{\text{OR, max}}$ for different values of incident peak power is calculated for each state of the memory cell (Fig. 3(a)). The results show a linear change of $V_{\text{OR, max}}$ versus the incident peak power. Such linear behavior is expected from OR effect and is consistent with the results provided in [36]. The results of our calculation also show a linear trend in changes of $\Delta V_{\text{OR, max}}$ while increasing the incident peak power (Fig. 3(b)). This in turn creates a quadratic trend for the potentially achievable memory readout rate, since it is proportional to square of $\Delta V_{\text{OR, max}}$.

Changing the dimensions of the STT-RAM array affects the strength of the aforementioned LSPR mode. This changes the values of $V_{\text{OR, max}}$. To study the effect of STT-RAM dimensions changes on the OR voltage, we fix the incident intensity to $3\,kW$ divided by the spot size ($20\,\mu m \times 20\,\mu m$). The main design dimensions are the cell diameter (d), thickness of the Au nanodisc (t_{Au}), and the unit cell period (p). For all the studies performed in this section, we fix the thickness of the Au plane to $t = 100\,nm$ which is much larger than the Au skin depth, and thickness of the CoFeB layers and the MgO layer to $t_{\text{CoFeB}} = 0.9\,nm$ and $t_{\text{MgO}} = 2\,nm$. We note that the thickness of the CoFeB layers and the MgO layer cannot be changed much, since they should stay in the typical range for efficient operation of the STT-RAM cells. However, since an asymmetry in the structure is shown to be a source of enhancement of OR voltage [17], at the end of this section we also study the effect of slight changes in the thickness of one of the CoFeB layers. This is to see if relative improvement in $\Delta V_{\text{OR, max}}$ can be achieved by the additional asymmetry created.

Changing the unit cell period of the STT-RAM array (p) has a direct effect on the efficiency of excitation of the plasmonic mode. By increasing p, the fill factor of the nanodiscs in the unit cell decreases, which results in a smaller peak absorption coefficient, as Fig. 4(a) shows (red curve). In addition, the resonance wavelength does not change with changing p, for values larger than a critical p value (the blue curve in Fig. 4(a)). This supports our claim that the excited plasmonic mode is an LSPR mode. Only for the case of $p = 150\,nm$, a slight red-shift in the resonance wavelength occurs, which is caused by the slight optical coupling between the memory cells. From memory readout point of view, our interest is in evaluating $\Delta V_{\text{OR, max}}$ in each memory cell, merely caused by the state change in that same cell, without being affected by the memory state of the adjacent cells. Therefore, a larger value of period should be selected to avoid such coupling.

Although the absorption peak decreases by increasing p, which means weakening of plasmonic resonance, larger $\Delta V_{\text{OR, max}}$ values are observed for larger periods. This is because in our simulations, the incident intensity stays the same, as mentioned earlier. In other words, the incident power per unit cell is larger for a larger period, which in turn increases $\Delta V_{\text{OR, max}}$ (blue curve in Fig. 4(b)). To show this, one can normalize the value of $\Delta V_{\text{OR, max}}$ to the unit cell area, where a reducing trend with the increase of the period can be seen (green curve in Fig. 4(b)). On the other hand, increasing p leads to a smaller number of STT-RAM cells being illuminated at a time, since we assume a fixed beam spot size for our calculations.

The cell diameter (d) in the STT-RAM cell is the major decision-maker for the resonance wavelength, where increasing it results in a red shift (Fig. 5(a)). This is expected, since d determines the extent of confinement of the optical field in y direction, which is the major field component of the LSPR mode. Furthermore, an increase in d leads to a stronger plasmonic resonance (shown by absorption peak increase in Fig. 5(a)), which is due to larger fill factor of the nanodiscs. On the other hand, it also increases the cross section area of the nanodiscs, which has a reducing effect on $V_{\text{OR, max}}$, according to equation (1), where the cross section area is in the denominator. These two contradictory effects result in smaller $\Delta V_{\text{OR, max}}$ values for cell diameters larger and smaller than an optimal value ($d = 100\,nm$ as shown in Fig. 5(b)). Similar trend is expected for the potentially achievable readout rate.

Changing the Au nanodisc thickness (t_{Au}) has an effect on the excitation of the LSPR mode as shown in Fig. 6(a), where a larger absorption peak can be observed for larger t_{Au} values, meaning a stronger plasmonic resonance. This increasing trend slows down as t_{Au} becomes larger. In addition, for t_{Au} values smaller than a critical value ($60\,nm$), a red shift in the resonance wavelength occurs (blue curve in Fig. 6(a)), which is due to the skin effect of gold. The enhancement of plasmonic excitation by increasing t_{Au} causes an increase in $\Delta V_{\text{OR, max}}$, while it follows a similar trend as the absorption

Authorized licensed use limited to: Access paid by The UC Irvine Libraries. Downloaded on December 07,2021 at 17:42:17 UTC from IEEE Xplore. Restrictions apply.

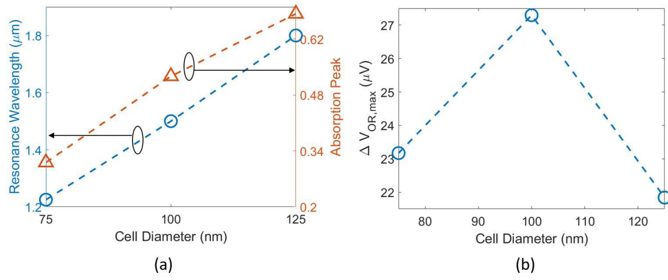

Fig. 5. Effect of changing the cell diameter of STT-RAM array on (a) Absorption peak and resonance wavelength (b) Maximum OR voltage change caused by the state change in each memory cell (STT-RAM array dimensions $p = 200\,nm$, $t_{\mathrm{Au}} = 60\,nm$, $t_{\mathrm{CoFeB}} = 0.9\,nm$, $t_{\mathrm{MgO}} = 2\,nm$, $t = 100\,nm$, incident peak power of $3\,kW$ and illumination beam spot size of $20\,\mu m \times 20\,\mu m$).

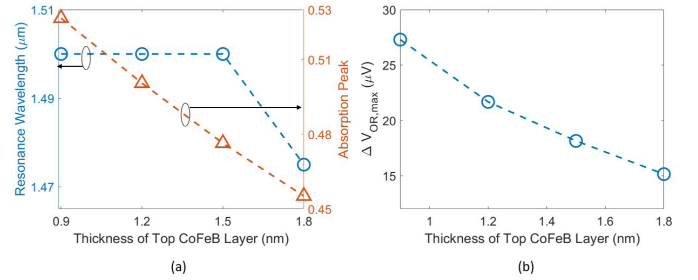

Fig. 7. Effect of changing the thickness of the top CoFeB layer of STT-RAM array on (a) Absorption peak and resonance wavelength (b) Maximum OR voltage change caused by the state change in each memory cell (STT-RAM array dimensions $p = 200\,nm$, $d = 100\,nm$, $t_{\mathrm{Au}} = 60\,nm$, $t_{\mathrm{CoFeB,\,bottom}} = 0.9\,nm$, $t_{\mathrm{MgO}} = 2\,nm$, $t = 100\,nm$, incident peak power of $3\,kW$ and illumination beam spot size of $20\,\mu m \times 20\,\mu m$).

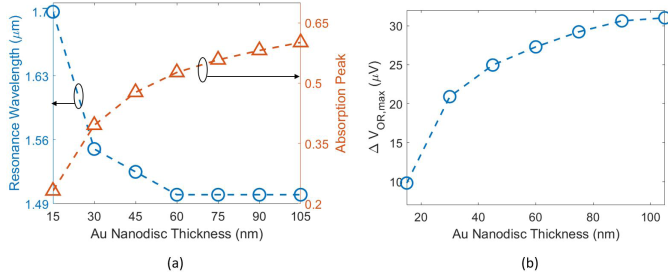

Fig. 6. Effect of changing the thickness of Au nanodisc of STT-RAM array on (a) Absorption peak and resonance wavelength (b) Maximum OR voltage change caused by the state change in each memory cell (STT-RAM array dimensions $p = 200\,nm$, $d = 100\,nm$, $t_{\mathrm{CoFeB}} = 0.9\,nm$, $t_{\mathrm{MgO}} = 2\,nm$, $t = 100\,nm$, incident peak power of $3\,kW$ and illumination beam spot size of $20\,\mu m \times 20\,\mu m$).

peak. This is shown in Fig. 6(b), where the $\Delta V_{\mathrm{OR,\,max}}$ value converges to $\sim 31\,\mu V$ for $t_{\mathrm{Au}} = 105\,nm$.

Finally, we study the effect of changing the thickness of one of the CoFeB layers, to see if the asymmetry caused by it can provide further enhancement of $\Delta V_{\mathrm{OR,\,max}}$. To do so, we slightly increase the thickness of the top CoFeB layer ($t_{\mathrm{CoFeB,\,top}}$) from $0.9\,nm$ to $1.8\,nm$ (staying in the range of typical CoFeB thicknesses for STT-RAM), while fixing the thickness of the bottom CoFeB layer at $t_{\mathrm{CoFeB,\,top}} = 0.9\,nm$. We calculate the absorption spectra as well as OR voltage change for different values of $t_{\mathrm{CoFeB,\,top}}$. The results are shown in Fig. 7. A reduction of absorption peak is observed when increasing $t_{\mathrm{CoFeB,\,top}}$, which is due to the losses of CoFeB. As the rest of the plots in Fig. 7 show, a thicker top CoFeB layer causes reduction of $\Delta V_{\mathrm{OR,\,max}}$, resulting in a decrease in potentially achievable readout rate. This means that the effect of losses introduced by the extra thickness of the top CoFeB layer is dominant, and no enhancement of $V_{\mathrm{OR,\,max}}$ occurs by introducing such asymmetry in the structure. Similar results are obtained when changing the thickness of the bottom CoFeB layer while keeping the thickness of the top one constant, which are not included here to avoid redundancy.

V. Adding a Transparent Electrode Layer to STT-RAM Array

Once the STT-RAM array dimensions are selected to obtain a larger $\Delta V_{\mathrm{OR,\,max}}$ value, one also needs to consider the impact of transparent electrodes that will couple the V_{OR} to the rest of the electrical circuitry. The photonics part of the design is especially interested in the impact of electrodes made of materials like ITO placed on top of the Au nanodisc in the unit cell structure as shown in Fig. 8(a). The space between the ITO layer and the Au plane at the bottom of the memory cell is filled with SiO_2 to support the ITO layer. As for the dimensions of the STT-RAM array, we choose the set that provide the highest $\Delta V_{\mathrm{OR,\,max}}$ value based on the results given in the previous section (listed in the caption of Fig. 8). We use the ITO optical material data given in [37] and set its thickness to $10\,nm$ for our calculations here. Using the calculated voltages for the two states of memory cell, we obtain $\Delta V_{\mathrm{OR,\,max}}$ for different wavelengths. For calculation of the OR voltage across one memory cell, including the voltage induced in the ITO layer, electron density and the screening length of ITO are needed, which we set to $n^{(0)} = 10^{27}\,m^{-3}$ and $l_{\mathrm{TF}} = 1.4\,\mathrm{Å}$ [38].

Looking at the absorption spectrum of the structure and comparing it with the previous case where no ITO and SiO_2 are present (blue curves in Fig. 8(b)), a 30% increase in absorption peak is calculated, which means a stronger plasmonic resonance. This in turn increases the field localization around the MgO layer, and results in further enhancement of ΔV_{OR}. As it can be seen in Fig. 8(b) (red curve), the maximum value of ΔV_{OR} for this structure is $\sim 41\,\mu V$, which is $\sim 32\%$ larger than the case without ITO and SiO_2. Through further investigation of the data (results not included here), we have verified that such enhancement is mainly due to the added SiO_2 around the memory cell, and the ITO layer has a minor effect, which is due to its small absorption. We note that the plasmonic enhancement of ΔV_{OR} is $\sim$20 times compared to the off-resonance wavelength of $1.3\,\mu m$. This results in enhancement of the potentially achievable readout rate by more than 400 times.

It is important to mention that depending on how large the laser pulse repetition frequency is, the $41\mu V$ voltage difference achieved through our design can be too small for the reading error to be negligible in practice. Typically, for a reliable measurement given a MHz-range laser pulse repetition frequency, the voltage difference should be in the order of millivolts. By playing with the key parameters of plasmonics, which are shape and dimensions, one can increase the voltage levels. For instance, further increase of the OR voltage may be

Authorized licensed use limited to: Access paid by The UC Irvine Libraries. Downloaded on December 07,2021 at 17:42:17 UTC from IEEE Xplore. Restrictions apply.

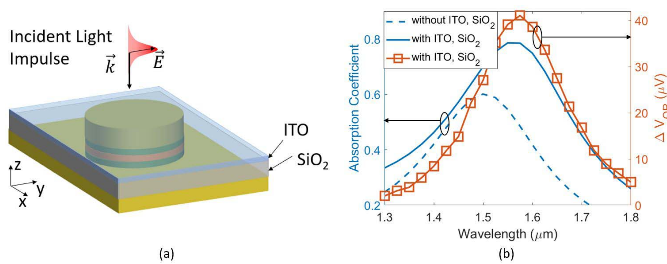

Fig. 8. (a) Schematic of STT-RAM array unit cell with added ITO electrode and SiO_2 (b) Absorption coefficient of the STT-RAM array with and without ITO and SiO_2 and the OR voltage change caused by the state change in each memory cell of the STT-RAM array with added ITO and SiO_2 (STT-RAM array dimensions $p = 200\,nm$, $d = 100\,nm$, $t_{\text{Au}} = 105\,nm$, $t_{\text{CoFeB}} = 0.9\,nm$, $t_{\text{MgO}} = 2\,nm$, $t = 100\,nm$, $t_{\text{ITO}} = 10\,nm$, incident peak power of $3\,kW$ and illumination beam spot size of $20\,\mu m \times 20\,\mu m$).

possible through implementation of other plasmonic structures, such as nanodisc dimers and bowtie antennas and optimizing their dimensions [20], [39].

VI. Discussion and Summary

When it comes to memory readout in practice, in addition to readout rate, it is important to study the possibility of unwanted switching of the memory cells due to readout. Under pulsed laser illumination, all-optical switching is known to occur through the so-called inverse Faraday effect, where magnetic coupling is induced by using a circularly polarized light, and thermal effects [40], [41]. In our case, we use linearly polarized light for the proposed readout method, which cannot create any magnetic moment to perform switching based on inverse Faraday effect. For linearly polarized light, however, thermal demagnetization can happen [42]. To estimate the impact of laser-induced heating in our design, we perform calculations based on illumination with a pulsed laser with $100\,MHz$ repetition rate and $1\,ps$ pulse width at $1550\,nm$. Considering our previous assumptions of $3\,kW$ peak power and $20\,\mu m \times 20\,\mu m$ beam area, pulse energy would be $3\,nJ$ for a rectangular pulse ($0.3\,pJ$ per cell). With these assumptions, we have performed a simplified numerical analysis using COMSOL Multiphysics 5.6, assuming Au instead of CoFeB and MgO layers in the cell structure shown in Fig. 8(a), using a rectangular pulsed heat source assuming 100 percent of the laser energy is converted into heat. Our model shows that the temperature increase due to laser heating is about $13\,K$, which is much lower than the Curie temperature of CoFeB thin film ($728\,K$ for a $1.1\,nm$-thick CoFeB film [43]). This means that the laser illumination in the proposed readout method is unlikely to demagnetize the free CoFeB layer in the STT-RAM cell and deteriorate its magnetic state. However, for an accurate estimate of the temperature, further study should be performed for a rigorous modeling which accounts for the effect of nanostructure shape, thermal resistance of the material interfaces, heat dissipation to the surrounding media, and transient dynamics of heating in the structure.

In conclusion, an opto-electronic readout method is proposed for parallel readout of STT-RAM cells, to simplify the readout circuitry without using conventional photodetectors. In this method, a single optical beam is utilized for illumination of an STT-RAM array, where the photo-induced voltage is assumed to be measured by conventional electronics. Such memory readout is performed based on optical rectification phenomenon, and enhancement of it is demonstrated through excitation of a localized plasmon resonance mode. Theoretical modeling of the structure is performed to calculate the photo-induced voltage in each memory cell in the array and the voltage variation with change of state in the memory cell. The effect of incident peak power and changes in dimensions of STT-RAM array on the photo-induced voltage and memory readout rate is studied. Furthermore, addition of an ITO layer as a transparent conductive electrode to facilitate probing of the photo-induced voltage is suggested and studied. Our model shows that in the proposed readout method, plasmonic enhancement helps increase the potentially achievable readout speed by more than 400 times.

References

[1] A. V. Krishnamoorthy, R. G. Rozier, J. E. Ford, and F. E. Kiamilev, "CMOS static RAM chip with high-speed optical read and write," *IEEE Photon. Technol. Lett.*, vol. 9, no. 11, pp. 1517–1519, Nov. 1997.

[2] D. Sanlyde, S. Skorobogatov, R. Anderson, and J.-J. Quisquater, "On a new way to read data from memory," in *Proc. 1st Int. IEEE Secur. Storage Workshop*, Dec. 2002, pp. 65–69.

[3] S. C. Li, J.-M. Lee, J. P. Su, and T.-H. Wu, "1.8-V nanospeed R/W module for 64-kB cross-point cell magnetic random access memory," *IEEE Trans. Magn.*, vol. 41, no. 2, pp. 909–911, Feb. 2005.

[4] Y. Chen, H. Li, X. Wang, W. Zhu, W. Xu, and T. Zhang, "A nondestructive self-reference scheme for spin-transfer torque random access memory (STT-RAM)," in *Proc. Design, Automat. Test Eur. Conf. Exhib. (DATE)*, Mar. 2010, pp. 148–153.

[5] A. Emboras *et al.*, "Nanoscale plasmonic memristor with optical readout functionality," *Nano Lett.*, vol. 13, no. 12, pp. 6151–6155, 2013.

[6] K. Zhang *et al.*, "VO_2-based selection device for passive resistive random access memory application," *IEEE Electron Device Lett.*, vol. 37, no. 8, pp. 978–981, Jun. 2016.

[7] O. Boyraz and B. Jalali, "Demonstration of a silicon Raman laser," *Opt. Exp.*, vol. 12, no. 21, pp. 5269–5273, 2004.

[8] H. Rong *et al.*, "An all-silicon Raman laser," *Nature*, vol. 433, no. 7023, pp. 292–294, Jan. 2005.

[9] Y. Wan *et al.*, "Monolithically integrated InAs/InGaAs quantum dot photodetectors on silicon substrates," *Opt. Exp.*, vol. 25, no. 22, pp. 27715–27723, 2017.

[10] L. Chen, K. Preston, S. Manipatruni, and M. Lipson, "Integrated GHz silicon photonic interconnect with micrometer-scale modulators and detectors," *Opt. Exp.*, vol. 17, no. 17, pp. 15248–15256, 2009.

[11] E. Garzón, R. De Rose, F. Crupi, L. Trojman, and M. Lanuzza, "Assessment of STT-MRAM performance at nanoscaled technology nodes using a device-to-memory simulation framework," *Microelectron. Eng.*, vol. 215, Jul. 2019, Art. no. 111009.

[12] K. L. Wang, J. G. Alzate, and P. K. Amiri, "Low-power non-volatile spintronic memory: STT-RAM and beyond," *J. Phys. D, Appl. Phys.*, vol. 46, no. 7, 2013, Art. no. 074003.

[13] M. Jasemi, S. Hessabi, and N. Bagherzadeh, "Reliable and energy efficient MLC STT-RAM buffer for CNN accelerators," *Comput. Electr. Eng.*, vol. 86, Sep. 2020, Art. no. 106698.

[14] L. Yang, Y. Cheng, Y. Wang, H. Yu, W. Zhao, and A. Todri-Sanial, "A body-biasing of readout circuit for STT-RAM with improved thermal reliability," in *Proc. IEEE Int. Symp. Circuits Syst. (ISCAS)*, May 2015, pp. 1530–1533.

[15] S. Yuasa, K. Hono, G. Hu, and D. C. Worledge, "Materials for spin-transfer-torque magnetoresistive random-access memory," *MRS Bull.*, vol. 43, no. 5, pp. 352–357, May 2018.

[16] T. Hatano, B. Nishikawa, M. Iwanaga, and T. Ishihara, "Optical rectification effect in 1D metallic photonic crystal slabs with asymmetric unit cell," *Opt. Exp.*, vol. 16, no. 11, pp. 8236–8241, 2008.

[17] H. Kurosawa, S. Ohno, and K. Nakayama, "Theory of the optical-rectification effect in metallic thin films with periodic modulation," *Phys. Rev. A, Gen. Phys.*, vol. 95, no. 3, Mar. 2017, Art. no. 033844.

Authorized licensed use limited to: Access paid by The UC Irvine Libraries. Downloaded on December 07,2021 at 17:42:17 UTC from IEEE Xplore. Restrictions apply.

[18] P. Sadri-Moshkenani *et al.*, "Plasmonic detection of possible defects in multilayer nanohole array consisting of essential materials in simplified STT-RAM cell," *Proc. SPIE*, vol. 10346, Aug. 2017, Art. no. 1034639.

[19] P. Sadri-Moshkenani *et al.*, "Array of symmetric nanohole dimers for STT-RAM ultrathin layer sensing," in *Proc. CLEO, Sci. Innov.*, 2019, pp. 1–2, Paper JW2A-60.

[20] P. Sadri-Moshkenani *et al.*, "Array of symmetric nanohole dimers with high sensitivity for detection of changes in an STT-RAM ultrathin dielectric layer," *J. Opt. Soc. Amer. B*, vol. 36, no. 11, pp. 3090–3097, 2019.

[21] N. Noginova, V. Rono, F. J. Bezares, and J. D. Caldwell, "Plasmon drag effect in metal nanostructures," *New J. Phys.*, vol. 15, no. 11, Nov. 2013, Art. no. 113061.

[22] M. Akbari, M. Onoda, and T. Ishihara, "Photo-induced voltage in nanoporous gold thin film," *Opt. Exp.*, vol. 23, no. 2, pp. 823–832, 2015.

[23] M. Durach and N. Noginova, "On the nature of the plasmon drag effect," *Phys. Rev. B, Condens. Matter*, vol. 93, no. 16, Apr. 2016, Art. no. 161406.

[24] M. Li, S. K. Cushing, and N. Wu, "Plasmon-enhanced optical sensors: A review," *Analyst*, vol. 140, no. 2, pp. 386–406, 2015.

[25] P. B. Johnson and R.-W. Christy, "Optical constants of the noble metals," *Phys. Rev. B, Condens. Matter*, vol. 6, no. 12, p. 4370, 1972.

[26] R. E. Stephens and I. H. Malitson, "Index of refraction of magnesium oxide," *J. Res. Nat. Bur. Standards*, vol. 49, no. 4, pp. 249–252, 1952.

[27] X. Liang, X. Xu, R. Zheng, Z. A. Lum, and J. Qiu, "Optical constant of CoFeB thin film measured with the interference enhancement method," *Appl. Opt.*, vol. 54, no. 7, pp. 1557–1563, 2015.

[28] V. Palenskis, "Drift mobility, diffusion coefficient of randomly moving charge carriers in metals and other materials with degenerated electron gas," *World J. Condens. Matter Phys.*, vol. 3, no. 1, pp. 78–81, 2013.

[29] J. Blakemore, "Electrons in metals," in *Solid State Physics*, 2nd ed. Cambridge, U.K.: Cambridge Univ. Press, 1985, pp. 149–292.

[30] S. Zhang, "Spin-dependent surface screening in ferromagnets and magnetic tunnel junctions," *Phys. Rev. Lett.*, vol. 83, p. 640, Jul. 1999.

[31] P. K. Amiri *et al.*, "Switching current reduction using perpendicular anisotropy in CoFeB–MgO magnetic tunnel junctions," *Appl. Phys. Lett.*, vol. 98, no. 11, 2011, Art. no. 112507.

[32] G. V. Swamy, P. K. Rout, M. Singh, and R. K. Rakshit, "Resistance minimum and electrical conduction mechanism in polycrystalline CoFeB thin films," *J. Phys. D, Appl. Phys.*, vol. 48, no. 47, Dec. 2015, Art. no. 475002.

[33] R. A. Matula, "Electrical resistivity of copper, gold, palladium, and silver," *J. Phys. Chem. Ref. Data*, vol. 8, no. 4, pp. 1147–1298, 1979.

[34] S. Ikeda *et al.*, "Dependence of tunnel magnetoresistance in MgO based magnetic tunnel junctions on Ar pressure during MgO sputtering," *Jpn. J. Appl. Phys.*, vol. 44, no. 48, pp. L1442–L1445, Nov. 2005.

[35] M. Durach, A. Rusina, and M. I. Stockman, "Giant surface-plasmon-induced drag effect in metal nanowires," *Phys. Rev. Lett.*, vol. 103, no. 18, Oct. 2009, Art. no. 186801.

[36] D. R. Ward, F. Hüser, F. Pauly, J. C. Cuevas, and D. Natelson, "Optical rectification and field enhancement in a plasmonic nanogap," *Nature Nanotechnol.*, vol. 5, no. 10, pp. 732–736, Oct. 2010.

[37] J. W. Cleary, E. M. Smith, K. D. Leedy, G. Grzybowski, and J. Guo, "Optical and electrical properties of ultra-thin indium tin oxide nanofilms on silicon for infrared photonics," *Opt. Mater. Exp.*, vol. 8, no. 5, pp. 1231–1245, May 2018.

[38] Z. Chen *et al.*, "High mobility indium tin oxide thin film and its application at infrared wavelengths: Model and experiment," *Opt. Exp.*, vol. 26, no. 17, pp. 22123–22134, 2018.

[39] R. Fernández-García, Y. Sonnefraud, A. I. Fernández-Domínguez, V. Giannini, and S. A. Maier, "Design considerations for near-field enhancement in optical antennas," *Contemp. Phys.*, vol. 55, no. 1, pp. 1–11, Jan. 2014.

[40] A. V. Kimel, A. Kirilyuk, P. A. Usachev, R. V. Pisarev, A. M. Balbashov, and T. Rasing, "Ultrafast non-thermal control of magnetization by instantaneous photomagnetic pulses," *Nature*, vol. 435, no. 7042, pp. 655–657, Jun. 2005.

[41] L. Avilés-Félix *et al.*, "Single-shot all-optical switching of magnetization in Tb/Co multilayer-based electrodes," *Sci. Rep.*, vol. 10, no. 1, pp. 1–8, Dec. 2020.

[42] C.-H. Lambert *et al.*, "All-optical control of ferromagnetic thin films and nanostructures," *Science*, vol. 345, no. 6202, pp. 1337–1340, Sep. 2104.

[43] M. Yamanouchi, A. Jander, P. Dhagat, S. Ikeda, F. Matsukura, and H. Ohno, "Domain structure in cofeb thin films with perpendicular magnetic anisotropy," *IEEE Magn. Lett.*, vol. 2, 2011, Art. no. 3000304.

Parinaz Sadri-Moshkenani received the M.S. degree in electrical engineering, communications, with a focus on fields and waves, from the University of Tehran in 2015. She is currently pursuing the Ph.D. degree with the University of California at Irvine, Irvine, CA, USA. During her Ph.D. studies, she also attended IMEC USA, FL, and ON Semiconductor, CA. Her research interests include optical sensing/imaging, plasmonics, and photonic integrated circuits.

Mohammad Wahiduzzaman Khan received the B.S. degree in electrical and electronic engineering from Bangladesh University of Engineering and Technology, Dhaka, Bangladesh, in 2014, and the M.S. degree in electrical and computer engineering from the University of California at Irvine, Irvine, CA, USA, in 2021, where he is currently pursuing the Ph.D. degree with the Department of Electrical Engineering and Computer Science. He has been working with the Advanced Photonic Devices and Systems Laboratory, UC Irvine, since 2016. His research interests include optical sensing, infrared detectors, integrated optics, and silicon photonics.

Md Shafiqul Islam received the B.Sc. degree from Bangladesh University of Engineering and Technology and the master's degree from the University of California at Irvine, Irvine, USA, where he is currently pursuing the Ph.D. degree. He is experienced in working in a LIDAR company as an Intern. His research interests include metalens and integrated photonic circuit design.

Eric Arturo Montoya received the B.S. degree from Western Washington University and the Ph.D. degree from Simon Fraser University. He is currently a Post-Doctoral Scholar with the University of California at Irvine, Irvine, USA. He is also a Magnetician and an Experimental Physicist whose research focuses on the interplay between magnetization dynamics and spin current, particularly in nanoscale systems where size, quantum, and topological effects can lead to emergent phenomena. In addition to fundamental research, he is interested in the utilization of these effects for practical spintronic applications, such as spin logic and memory and quantum, neuromorphic, and reservoir computing.

Ilya Krivorotov (Senior Member, IEEE) received the Ph.D. degree in physics from the University of Minnesota in 2002. He was a Post-Doctoral Associate with Cornell University, before joining the University of California at Irvine, Irvine, USA, as a Faculty Member, in 2005. He is currently a Professor of physics with UC Irvine. The focus of his research is physical phenomena resulting from the interactions between magnetic, electronic and lattice degrees of freedom in solids and their device applications. Examples of such research include spin currents and spin torques in ferromagnetic nanostructures, spin torque memory technologies (STT-MRAM and SOT-MRAM), spin torque oscillators, spin wave devices, spin caloritronics, magneto-electric effect in nanostructures, and proximity effect in ferromagnet/superconductor systems. He is a fellow of the American Physical Society. He was a recipient of the NSF CAREER Award.

Ozdal Boyraz received the M.S. and Ph.D. degrees from the University of Michigan, Ann Arbor, in 1997 and 2001, respectively. After two years of industrial experience at Xtera Communications, Allen, TX, USA, he joined the University of California at Los Angeles, Los Angeles, USA, as a Post-Doctoral Research Fellow, in 2003, where he joined the Electrical Engineering Department, as a tenure-track Faculty, in 2005. He has over 200 journal and conference publications and holds six issued patents. His research areas include silicon-based optoelectronic devices, nanophotonics, optical communications systems, RF over fiber, nonlinear optics, and optical signal processing. He is a Senior Member of OSA. He was a recipient of the 2010 DARPA Young Faculty Award.

Authorized licensed use limited to: Access paid by The UC Irvine Libraries. Downloaded on December 07,2021 at 17:42:17 UTC from IEEE Xplore. Restrictions apply.